Nonlinear focusing of acoustic shock waves at a caustic cusp

Régis Marchiano[a] and François Coulouvrat
Laboratoire de Modélisation en Mécanique, Université Pierre et Marie Curie and CNRS (UMR 7607), 4 place Jussieu, 75252 Paris Cedex 05, France

Jean-Louis Thomas
Laboratoire des Milieux Désordonnés et Hétérogènes, Université Pierre et Marie Curie and CNRS (UMR 7603), 4 place Jussieu, 75252 Paris Cedex 05, France

(Received 4 May 2004; revised 27 October 2004; accepted 7 November 2004)

The present study investigates the focusing of acoustical weak shock waves incoming on a cusped caustic. The theoretical model is based on the Khokhlov–Zabolotskaya equation and its specific boundary conditions. Based on the so-called Guiraud's similitude law for a step shock, a new explanation about the wavefront unfolding due to nonlinear self-refraction is proposed. This effect is shown to be associated not only to nonlinearities, as expected by previous authors, but also to the nonlocal geometry of the wavefront. Numerical simulations confirm the sensitivity of the process to wavefront geometry. Theoretical modeling and numerical simulations are substantiated by an original experiment. This one is carried out in two steps. First, the canonical Pearcey function is synthesized in linear regime by the inverse filter technique. In the second step, the same wavefront is emitted but with a high amplitude to generate shock waves during the propagation. The experimental results are compared with remarkable agreement to the numerical ones. Finally, applications to sonic boom are briefly discussed.
[DOI: 10.1121/1.1841551]

PACS numbers: 43.25.Cb, 43.25.Jh, 43.28.Mw [MFH] Pages: 566–577

I. INTRODUCTION

The focusing of finite amplitude waves on a cusped caustic is a physical phenomenon which may occur in different circumstances: sonic boom focusing produced either by the aircraft's manoeuvres or by the atmospheric turbulence or wavefront distortion encountered in medical imaging or nondestructive evaluation through heterogeneous medium. For all cases, it is important to better understand and control this phenomenon in order to either avoid it (sonic boom) or take benefits from it (imaging or nondestructive evaluation).

A caustic is an envelope of rays. It corresponds to a surface of amplification of the wavefield. There exist different kinds of caustics: fold, cusp, swallow-tail, and so on. All of these are described and classified by the theory of catastrophes (Thom, 1972). An important result of this theory is that for a wavefield, caustics can be interpreted as structurally stable focuses (Berry, 1976). In this framework, the perfect point focus is unstable and is likely to degenerate into a stable caustic such as a cusped caustic. Moreover, the theory of catastrophes also provides the generic form for the high frequency limit of the pressure field around the caustics in the linear regime, where diffraction cannot be neglected and is the main physical mechanism. This is the reason why this theory is also called the diffraction theory of catastrophes (Berry, 1976). For a cusped caustic this analytical solution is the Pearcey function (Pearcey, 1946). The reader is referred to Marston (1992) for a review of acoustical caustics in linear regime (with smooth waves).

If the incoming waves are shock waves, the Pearcey function is not valid because it predicts peaks of infinite amplitude on the cusped caustic (Coulouvrat, 2000). Note that this problem presents many analogies with the problem of the fold caustic for which the analytical solution—the Airy function—also leads to an infinite amplitude if the incoming waves present shocks (Guiraud, 1965). This is obviously physically meaningless, and experimental investigations performed during flight tests (Wanner *et al.*, 1972; Downing *et al.*, 1998) or laboratory experiments (Davy and Blackstock, 1971; Sanai *et al.*, 1976; Sturtevant and Kulkarny, 1976), despite an important amplification of amplitude and a change in the temporal waveform associated to diffraction, clearly show a limitation of the amplitude. Guiraud (1965) was the first to propose nonlinearities as the additional limiting mechanism for the case of fold caustics. He derived the so-called nonlinear Tricomi equation satisfied by the pressure field around the caustic. An approximate numerical solution was designed by Gill and Seebass (1973) based on the hodograph transform, and recently a fully numerical solution has been developed (Marchiano *et al.*, 2003a). Estimations by Plotkin and Cantril (1976) and later by Downing *et al.* (1998) showed the Gill and Seebass solution matched reasonably well with flight tests, while Marchiano *et al.* (2003b) demonstrated nice agreement with numerical solutions of Guiraud's model by means of a carefully scaled experiment in water tank.

For cusped caustics, in order to estimate the amplitude of the pressure at the tip of a cusped caustic, Pierce (1971) derived a similarity rule stipulating that the amplitude varies as the power $\frac{2}{3}$ of the incoming shock wave. But that result is valid for an incoming step function only. Using the asymptotic method of matched expansions, Cramer and See-

[a]Electronic mail: marchi@lmm.jussieu.fr

bass (1978) showed that around the cusped caustic, the pressure is governed by the Khokhlov–Zabolotskaya equation (Zabolotskaya and Khokhlov, 1969). That first model, valid for a 2D homogeneous medium, has been extended to the 3D case (Cramer, 1981a) and to the case of an axisymetric arête (Cramer, 1981b). In accordance with Guiraud's assumptions on the fold caustic (Guiraud, 1965) and with the theory of catastrophes, Coulouvrat (2000) showed that it is possible to derive the KZ equation considering a boundary layer around the cusp where the main physical mechanisms are diffraction and local nonlinear effects. Moreover, he derived the full associated boundary conditions which make it possible to solve the problem numerically for any incoming waveform.

In this paper, after a brief recall of the modeling associated with a cusped caustic (Sec. II), a detailed discussion about the Guiraud similitude laws for a cusped caustic, derived by Coulouvrat (2000), is presented (Sec. III). In particular, the wavefront unfolding observed by Piacsek (2002) is examined with both theoretical and numerical approaches, and a new mechanism for explaining it is proposed. However, numerical tests are not sufficient by themselves to conclude about the validity of the assumptions of the theoretical modeling, and an experimental confirmation is required, as presented in Sec. IV using ultrasonic shock waves in a water tank (Sec. IV). To our knowledge, this is the first time that theory and experiments have been compared quantitatively. This approach allows us to confirm definitively the assumptions of the theory and to validate the computer code.

II. THEORETICAL BACKGROUND: THE KZ EQUATION

In a two-dimensional, homogeneous and inviscid fluid of sound speed c_0, we consider the propagation of a concave wavefront having at point O (chosen as the origin) a minimum of radius of curvature, noted R_0. In the present section, it is assumed the wavefront is part of a continuous wave with angular frequency ω and wave number $k_0=\omega/c_0$. The case of a shock front will be discussed in next section. The x axis is chosen tangent to, and the z axis normal to, the wavefront at the origin (Fig. 1). During the propagation, that wavefront generates a cusped caustic at the distance R_0 from the origin. The wavefront having a minimum of the radius of curvature, the tip of the caustic is oriented towards the origin. The cusped caustic splits the space into two distinct zones (Fig. 1): one, labeled zone I, where only one ray passes through each point (area located outside the branches of the caustic), and one, labeled zone II, where three rays pass through each point (area located within the branches of the caustic).

Introducing the geometrical parameter $a=\frac{9}{8}R_0^2R_0^{\parallel}$, where $R_0^{\parallel}$ is the second derivative with respect to x at the origin O, Coulouvrat (2000) defines the characteristic diffraction length-scale in the z direction:

$$L_z=\left(\frac{4a}{27k_0}\right)^{1/2}, \tag{1}$$

and the characteristic diffraction length-scale in the x direction:

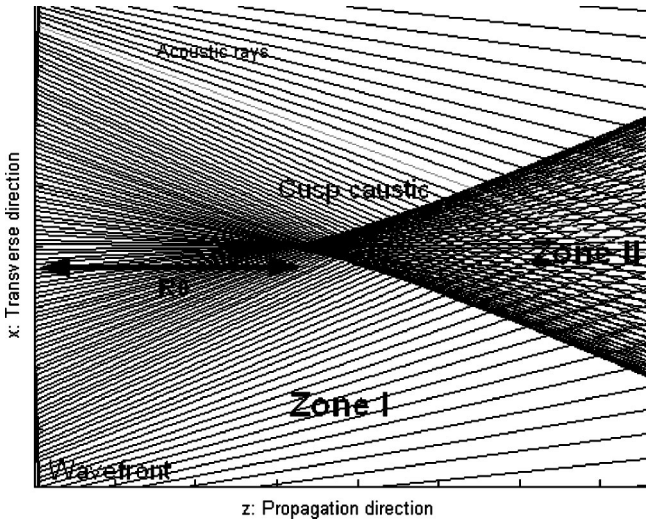

FIG. 1. Geometry of the caustic. Note that, in order to emphasize the caustic geometry, the scales of the transverse and propagation directions are not the same.

$$L_x=\left(\frac{a}{27k_0^3}\right)^{1/4}. \tag{2}$$

The diffraction length-scales are used to define the spatial dimensionless variables characterizing the problem in the longitudinal direction,

$$\overline{z}=(z-R_0)/L_z, \tag{3}$$

and in the transverse direction,

$$\overline{x}=x/L_x. \tag{4}$$

The dimensionless retarded time is also introduced to describe propagation in the main direction, t being the physical time:

$$\overline{t}=\omega(t-z/c_0). \tag{5}$$

Lastly, the dimensionless pressure is introduced:

$$\overline{p}=\frac{p}{p_0}, \tag{6}$$

where p is the acoustical pressure and p_0 is chosen as the amplitude of the incoming pressure field before focus at one characteristic distance L_z (the amplitude at $\overline{z}=-1$).

Cramer and Seebass (1978) and Coulouvrat (2000) show that, in the neighborhood of the cusp, the pressure is solution of the Khokhlov–Zabolotskaya equation (KZ equation):

$$\frac{\partial^2\overline{p}}{\partial\overline{z}\partial\overline{t}}=\frac{\partial^2\overline{p}}{\partial\overline{x}^2}+\mu\frac{\partial^2\overline{p}^2}{\partial\overline{t}^2}, \tag{7}$$

where μ is a parameter measuring the amplitude of the nonlinear effects in comparison with diffraction ones:

$$\mu=\beta M\left(\frac{k_0a}{27}\right)^{1/2}=\beta\frac{p_0}{\rho_0c_0^2}\left(\frac{k_0a}{27}\right)^{1/2}, \tag{8}$$

with $\beta=1+B/2A$ (where $B/2A$ is the nonlinearity parameter of the medium) and $M=p_0/\rho_0c_0^2$ the acoustical Mach number (where ρ_0 is the density of the medium at rest).

The boundary conditions associated with the problem are determined by an asymptotic matching with the geometrical acoustics away from the cusp (Coulouvrat, 2000):

$$\overline{p}(\overline{x},\overline{z},\overline{t}) \xrightarrow[\sqrt{\overline{x}^2+\overline{z}^2}\to\infty]{} \frac{1}{\sqrt{|6\overline{\alpha}^2-\overline{z}|}}F(\overline{t}+\overline{\alpha x}+\overline{\alpha}^2\overline{z}-\overline{\alpha}^4), \quad (9)$$

where $\overline{\alpha}(\overline{x},\overline{z})$ is the only real root of $\overline{x}+2\overline{\alpha z}-4\overline{\alpha}^3=0$ and F is the dimensionless incoming signal waveform. The phase function $\overline{t}+\overline{\alpha x}+\overline{\alpha}^2\overline{z}-\overline{\alpha}^4$ describes the curvature of the wavefront as it approaches the caustic, while the coefficient $1/\sqrt{|6\overline{\alpha}^2-\overline{z}|}$ measures the subsequent geometrical amplification. This expression is valid only in zone I (Fig. 1), where only one ray [one root $\overline{\alpha}(\overline{x},\overline{z})$] passes through each point, and sufficiently far from the caustics so that local diffraction effects can be neglected (geometrical approximation).

The boundary condition Eq. (9) completes the formulation of the problem and makes it numerically tractable. For the linear case ($\mu=0$), Coulouvrat (2000) shows that the solution of Eqs. (7) and (9) can be expressed in terms of the Pearcey function (1946), in agreement with the diffraction catastrophe theory (Berry, 1976; Marston, 1992). For the nonlinear case, a new algorithm solving the KZ equation is presented in Appendix A.

III. GUIRAUD'S SIMILITUDE FOR A STEP SHOCK

We briefly recall here the similitude law obtained by Cramer and Seebass (1978) and Coulouvrat (2000) generalizing to a cusped caustic the Guiraud's similitude (1965) for a fold caustic. Introducing the new scaling $\overline{p}=\mu^{-1/3}\tilde{p}$, $\overline{t}=\mu^{4/3}\tilde{t}$, $\overline{x}=\mu\tilde{x}$, $\overline{z}=\mu^{2/3}\tilde{z}$ and $\overline{\alpha}=\mu^{1/3}\tilde{\alpha}$, the KZ equation becomes

$$\frac{\partial^2\tilde{p}}{\partial\tilde{z}\partial\tilde{t}}=\frac{\partial^2\tilde{p}}{\partial\tilde{x}^2}+\frac{\partial^2}{\partial\tilde{t}^2}(\tilde{p}^2), \quad (10)$$

and the associated boundary condition

$$\tilde{p}(\tilde{x},\tilde{z},\tilde{t})\approx\frac{1}{\sqrt{|\tilde{z}-6\tilde{\alpha}^2|}}F[\mu(\tilde{t}+\tilde{\alpha}\tilde{x}+\tilde{\alpha}^2\tilde{z}-\tilde{\alpha}^4)] \quad (11)$$

with $\tilde{\alpha}$ the only real root of the polynomial $\tilde{x}+2\tilde{\alpha}\tilde{z}-4\tilde{\alpha}^3=0$.

With the new scaling, the KZ equation [Eq. (10)] no longer involves the nonlinear parameter μ which now appears in the boundary conditions [Eq. (11)]. Thus, for an incoming step shock which is invariant by temporal dilatation [$F(\overline{t})=0$ if $\overline{t}<0$ and $F(\overline{t})=1$ if $\overline{t}>0$], the whole problem [Eqs. (10) and (11)] is independent of the nonlinear parameter: this is a self-similar solution (with respect to the nonlinear parameter), known as Guiraud's similitude. Expressing the similitude variables "$\sim$" in physical terms, one finds

$$\tilde{p}=p\left[\frac{\beta}{\rho_0c_0^2p_0^2}\left(\frac{k_0a}{27}\right)^{1/2}\right]^{1/3}.$$

However, the amplitude p_0 is defined as the incoming pressure amplitude at one boundary layer thickness away from the cusp. But for a step shock, there is no main frequency, therefore the choice of this thickness is arbitrary. Taking into account the convergence of the pressure field according to the boundary condition Eq. (9), it is therefore suitable to write $p_0=P_{ref}(a/L_z)^{1/2}$, where P_{ref} is a reference pressure level now independent of the frequency (a being now the only physical length of the problem). This finally yields

$$\tilde{p}=p\left[\frac{2\beta}{27\rho_0c_0^2P_{ref}^2}\right]^{1/3} \quad (12)$$

and results for other variables can be deduced similarly:

$$\begin{aligned}
&\tilde{t}=\frac{6}{2^{1/3}}\left(\frac{\rho_0c_0^2}{\beta P_{ref}}\right)^{3/4}\frac{c_0}{a}(t-z/c_0),\\
&\tilde{x}=54^{1/2}\left(\frac{\rho_0c_0^2}{\beta P_{ref}}\right)\frac{x}{a},\quad \tilde{z}=\frac{9}{4^{1/3}}\left(\frac{\rho_0c_0^2}{\beta P_{ref}}\right)^{2/3}\frac{z}{a},\\
&\tilde{\alpha}=2^{1/6}\sqrt{3}\left(\frac{\rho_0c_0^2}{\beta P_{ref}}\right)^{1/3}\frac{\alpha}{R_0}.
\end{aligned} \quad (13)$$

Relations (12) and (13) are all independent of frequency, indicating that Guiraud's scaling is the correct one for an incoming signal with no characteristic frequency. As a counterpart, the scaling is nonlinear. Especially, Eq. (12) shows that the focused pressure varies as power $\frac{2}{3}$ of the incoming amplitude, in agreement with Pierce's (1971) dimensional analysis later confirmed by Cramer and Seebass (1978). The characteristic space variables increase as power $\frac{2}{3}$ of the amplitude along the axis, and power 1 transversely, while characteristic time increases as power $\frac{3}{4}$.

Guiraud's similitude is the key point in solving the issue of weak shocks focusing. Whitham (1956) conjectured that the nonlinear self-refraction prevents wavefront folding as the central part of the shock front tends to become plane. That is the mechanism of "wavefront unfolding." This view point, also supported by Marston (1988), has been numerically investigated by Prasad and Sangeeta (1999) using a weak nonlinear ray theory but for Mach numbers (from 1.05 to 1.2) significantly larger than acoustical ones. This seems contradictory to Guiraud's similitude, which *demonstrates* (provided the basic assumptions sustaining the KZ equation are valid, as will be demonstrated in Sec. IV) that the solution is independent of the amplitude after correct rescaling, at least in the weak shock approximation of the KZ equation. Experiments by Sturtevant and Kulkarny (1976, Figure 17) confirm that for weak shock waves (Mach 1.005 and 1.03), the geometrical shape of the wavefront remains such that there is no self-refraction, though for stronger shocks beyond the acoustical limit (Mach 1.1 and 1.5) this is no longer valid. On the contrary, using numerical simulations of the NPE equation, Piacsek (2002) observes wavefront unfolding even in the acoustical limit. But for the "ideal" wavefront Eq. (9) leading to a "perfect" cusped caustic, Guiraud's similitude demonstrates that this should not happen.

To elucidate this issue, we have performed numerical simulations of the two cases: first for the "ideal" wavefront Eq. (9) exactly associated to Pearcey solution in the linear regime, and for the wavefront proposed by Piacsek [his equation (5)]. This last wavefront involves two parameters. These ones have been chosen so that both wavefronts have the

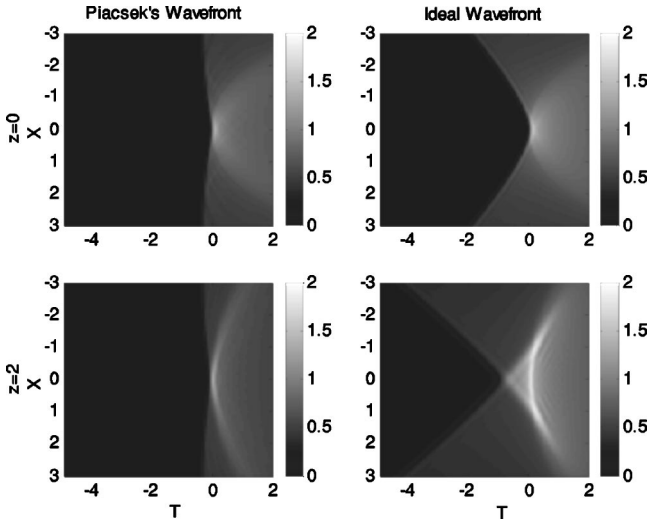

FIG. 2. Numerically simulated dimensionless pressure fields $\overline{p}$ at $\overline{z}=0$ and $\overline{z}=2$ in linear regime ($\mu=0$) as a function of time (horizontal) and transverse space variable $\overline{x}$ (vertical) for a step shock. Vertical bar indicates correspondance between gray and dimensionless pressure levels. Comparison between Piacsek's ''real'' wavefront (left column) and ''ideal'' wavefront Eq. (9) (right column).

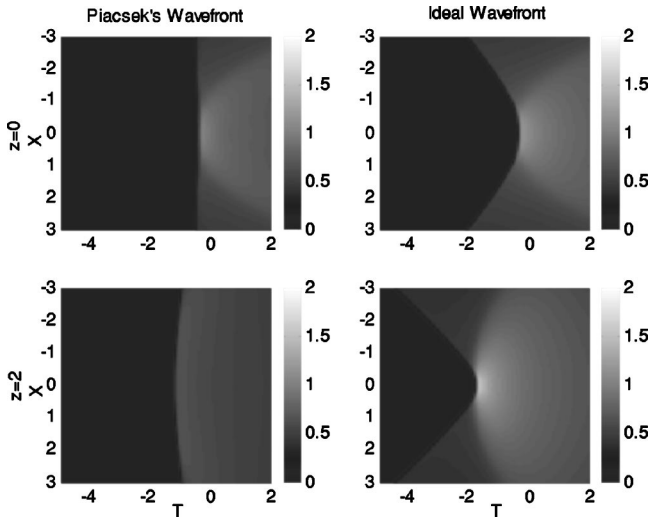

FIG. 3. Numerically simulated dimensionless pressure fields $\overline{p}$ at $\overline{z}=0$ and $\overline{z}=2$ in nonlinear regime ($\mu=1$) as a function of time (horizontal) and transverse space variable $\overline{x}$ (vertical) for a step shock. Vertical bar indicates correspondance between gray and dimensionless pressure levels. Comparison between Piacsek's ''real'' wavefront (left column) and ''ideal'' wavefront Eq. (9) (right column).

same values R_0 and $R_0^{\parallel}$ at their center. So, locally, the two wavefronts have the same geometry. Therefore, according to catastrophe theory, in the high frequency limit and in the linear regime, the two are locally equivalent around the cusp of the caustic. However, far from the center, the ''ideal'' one, Eq. (9), is still converging with a shape perfectly suited to a cusped caustic, while Piacesk'one gets flat, and is therefore not focusing any more.

The numerical simulations are performed for a step shock using a new code solving the KZ equation in the temporal domain (see the Appendix for further technical details and code validation). Piacsek' wavefront is used in the initial plane $z=0$. Laterally, the solution is matched to an analytical solution of the inviscid Burgers' equation (nonlinear plane wave). Results of the simulations are shown in linear regime ($\mu=0$ in the KZ equation) on Fig. 2. The two wavefronts clearly focus at $\overline{z}=0$ with the same amplitude. Beyond this point, they exhibit the characteristic swallow tail form at $\overline{z}=2$. Note, however, that the focusing effects are much more localized for Piascek's wavefront, as far from the axis it is not focusing any more. In nonlinear regime ($\mu=1$, Fig. 3), the results are quite different. The ''ideal'' wavefront Eq. (9) always leads to form a cusped caustic but now the focus is strongly shifted, around point $\overline{z}=2$ (very similar to the curve for $\overline{z}=0$ in linear regime). On the contrary, the Piascek's wavefront is flattened, an effect already described by Piacsek (2002). Note that nonlinear effects are visible for both cases: the time when the step shock (in $\overline{x}=0$) occurs is no longer zero but shifted to an earlier time for higher amplitude.

As soon as the wavefront deviates from the ''ideal'' wavefront Eq. (9), there is some critical amplitude beyond which the current shape of the wavefront (which has all chances to deviate at some distance from the ideal one) plays a role. Indeed, as the pressure amplitude increases, Guiraud's self-similar solution requires rays from a larger region of the wavefront [Eq. (13) for α, increasing as power $\frac{1}{3}$ of the amplitude]. So, if the transverse size of the wavefront where it is close to the ideal one is not large enough, the cusped caustic cannot be actually synthesized in nonlinear regime. This is equivalent to the linear catastrophe theory (leading to the Pearcey function), which is a local, high frequency approximation. When wavelength increases, this approximation degrades or conversely the size of the wavefront should be increased. Here, the phenomenon is analogous, but the wavelength increase is associated with the nonlinear increase of the characteristic length scales of Guiraud's similitude with the amplitude. Consequently, beyond some amplitude, any real wavefront will deviate from the Guiraud's similitude, which will appear as a wave front unfolding. So the conclusion is that there is indeed wave front unfolding, but it is not intrinsically a nonlinear phenomenon (at least for acoustic shock waves). It is a more complex process, where the self-similar solution of Guiraud becomes invalid with increasing amplitudes because the characteristic lengths increase with amplitude, so that the actual shape of the wavefront (and not only its local asymptotic shape) gets more and more important.

IV. EXPERIMENTAL SYNTHESIS OF A CUSPED CAUSTIC

In order to verify the assumptions of the theory, an experimental study has been performed. The experiments are made in a water tank with ultrasonic waves (central frequency: 1 MHz) emitted by an array of 256 rectangular piezoelectric transducers (Imasonic, France). The transducers are displayed on a rectangular aperture (32 rows, 8 lines). Each of them is driven individually by programmable broadband linear amplifiers (Lecoeur Electronique, France). Those amplifiers allow us to specify the shape, phase and amplitude of the signal emitted by a transducer. Each transducer can emit a plane wave up to 5×10^5 Pa amplitude. A broadband calibrated membrane hydrophone (1 to 40 MHz) associated

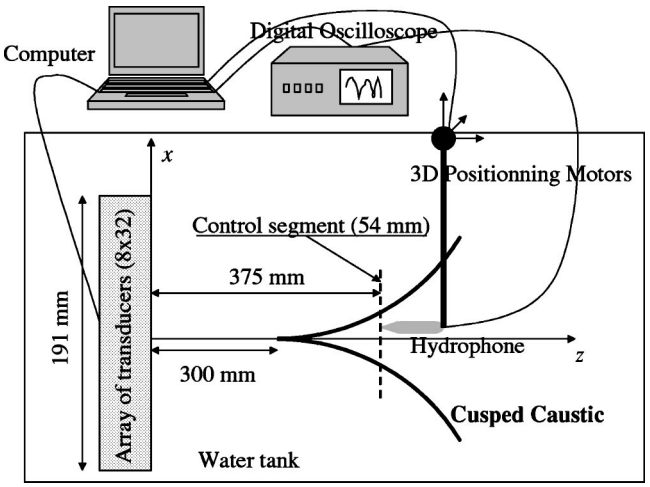

FIG. 4. Experimental setup.

with a digital oscilloscope measures the acoustic field. The small active diameter of the hydrophone (0.2 mm), ensures a good resolution to scan the acoustic field. The hydrophone can be moved along the three directions of space inside the water tank by programmable step-by-step motors (Fig. 4). The whole experimental setup is automated.

The experimental synthesis of a cusped caustic in linear and nonlinear regimes presented here is achieved in two stages. First of all, the signals to be emitted by the array in order to synthesize a cusped caustic in linear regime are determined. That stage is achieved by the inverse filter technique (Tanter *et al.*, 2000). Once the signals producing the cusped caustic are known, the second stage consists in emitting them with a high amplitude to produce nonlinearity. This methodology has been employed successfully to synthesize fold caustics in the nonlinear regime (Marchiano *et al.*, 2003b).

The geometrical parameters of the cusp are chosen as follows: $R_0=300$ mm and $R_0^{\|}=63/R_0$. With the choice of the propagation medium (water, $c_0\approx 1500$ m/s) and the frequency of the waves ($f_0=1$ MHz), the choice of the values of R_0 and $R_0^{\|}$ fixes the geometry of the problem, and in particular the diffraction length-scales: $L_z=27.4$ mm in the propagation direction and $L_x=1.8$ mm in the transverse direction. This choice results from the compromise between the size of the focal length and the distance between the array of transducers and the tip of the caustic. The latter distance must be large enough to ensure the presence of shock waves. The shock formation distance for a plane wave emitted by the array of transducers is about 300 mm. Nevertheless, this distance is shorter in the case of a focused wave such as the emitted wave. So, the chosen distance (300 mm) is sufficiently far from the array to ensure the presence of shock wave. Figure 5 shows the acoustical rays launched by an unlimited [Fig. 5(a)] and a limited [Fig. 5(b)] wavefront producing the cusped caustic with the geometrical parameters R_0 and $R_0^{\|}$ defined above. The size of the limited wavefront corresponds to the aperture of the array of transducers used for the experiments (191 mm). On both figures, the cusped caustic appears clearly, especially the tip of the cusp located 300 mm away from the wavefront (the array). As

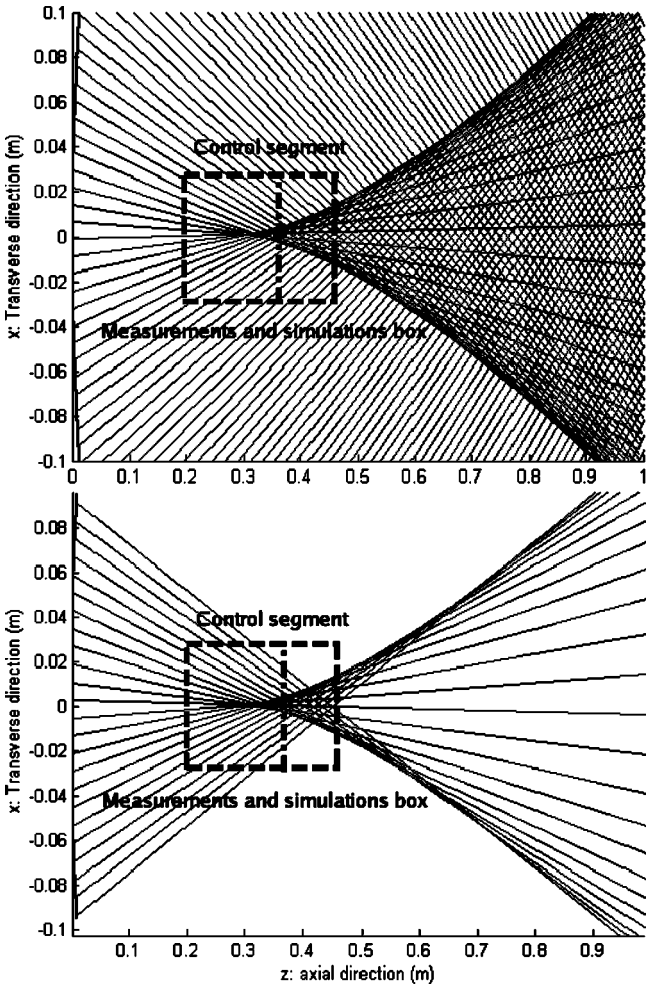

FIG. 5. Acoustical rays launched by (a) an unlimited and (b) a limited aperture. Note that the scales of the transverse and propagation directions are not the same. The dotted box indicates the domain where measurements and simulations are performed. The dotted line represents the position of the control segment.

mentioned in Sec. I, for an unlimited wavefront, the cusped caustic splits the plane Oxz into two zones: a zone with one ray and a zone with three rays. For a limited aperture, the situation is different. Three zones can be distinguished: a zone with no ray, a zone with one ray, and a zone with three rays. Nevertheless, near the tip of the cusp, the field is identical to the modeled phenomenon. That zone corresponds to the area where the theory described in Sec. 1 is valid and where we can make comparison between theory and experiment.

To synthesize the cusped caustic in linear regime, the inverse filter technique is used. The first stage of this technique consists in measuring the propagation operator between the array of transducers and a set of control points, where the target field must be synthesized. The linear solution to the problem is the Pearcey function. So the target field is defined from that function, which depends on the two spatial variables x and z and is computed from the code presented in Sec. II with $\mu=0$. Because of technical considerations (size of the memory, duration of the experiment), we choose to impose the Pearcey function not on a plane (natural choice for a function of two variables) but along a seg-

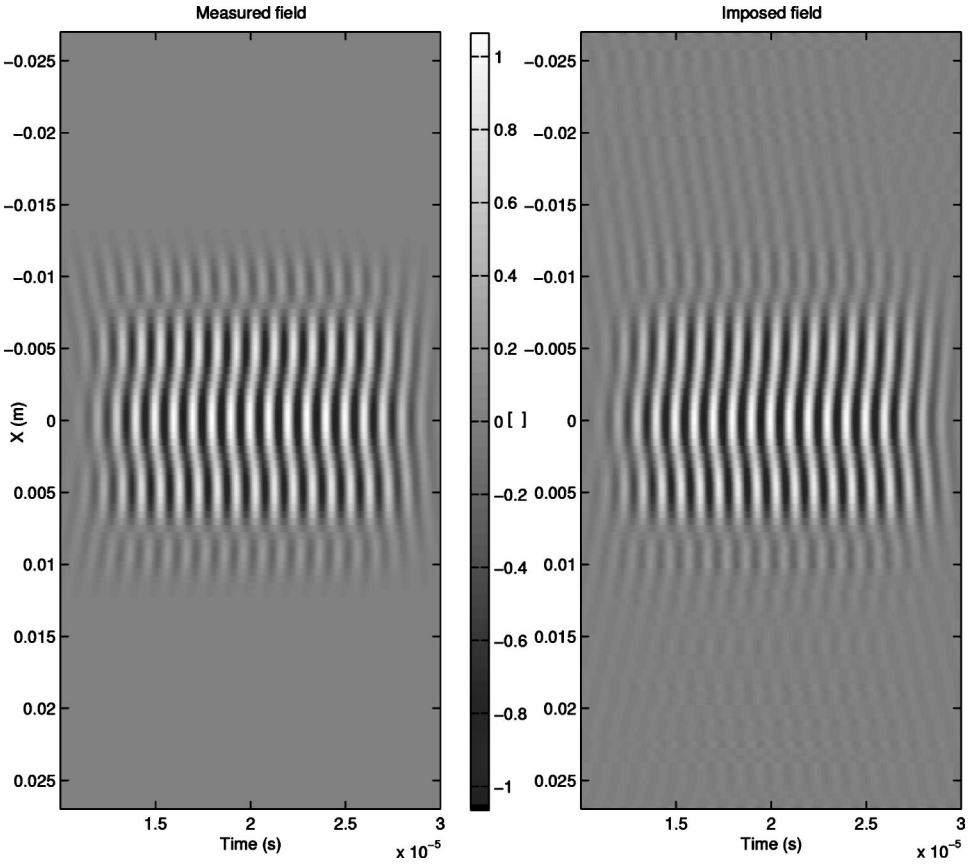

FIG. 6. Spatio temporal pressure field (a) imposed and (b) measured along the control segment (horizontal: time variable; vertical: transverse space variable; gray levels: pressure levels).

ment only. We define this control segment located 382 mm away from the array. Its length is 54 mm and it is discretized by 108 points equally spaced every 0.5 mm. The size and the location of the control segment have been chosen in order that the segment is behind the tip of the cusp and crosses the caustic so that it is located partially in zone I and partially in zone II. So, imposing the acoustic field on that segment makes the acoustic field strongly stressed. The propagation operator is measured between that control segment and the array of transducers. Then, the propagation operator is regularized and inversed by a singular value decomposition.

The incoming function used to compute the pattern (the Pearcey function) is a sinusoidal function with a dozen cycles. Nevertheless, such a computed field does not take into account the finite size of the array of transducers and corresponds to the ideal situation depicted on Fig. 5(a). To impose a realistic pattern on the control segment, a function is applied on the field previously computed. The windowing keeps the central part of the field and eliminates the lateral parts as illustrated on Fig. 6(a). This new pattern is used to calculate the signals to emit by the transducers. Then, those signals are emitted at low amplitude to ensure a linear propagation and the pressure is measured on the control points. Figure 6(b) shows the field measured along the control segment compared to the pattern imposed [Fig. 6(a)]. The agreement between the two fields is very good; the main characteristics of the target field are well recovered: the structure with three lobes and the shape of the wavefronts. This comparison proves that the field corresponding to a cusped caustic can be synthesized along a segment.

In order to confirm that the cusped caustic is synthesized in the whole space (and not only on the control segment) a scan on a bigger grid is achieved. The grid is 240 mm long in the z direction (100 mm before the tip and 140 mm after the tip, the step is 2 mm) and 54 mm large in the x direction (27 mm on each side of Oz axis, the step is 0.5 mm). So, there are 12 360 points on the new measurement grid (the limits of the grid are the dashed lines on Fig. 5). The pressure is measured with a temporal sampling of 50 MHz.

To compare the experimental measurements to the numerical simulations discussed in Sec. II, only the incoming waveform is necessary as an input argument. This data is extracted directly from the experimental measurements 100 mm away from the tip of the cusp on the propagation axis Oz. In order to perform comparisons with the experimental results, the pressure field is computed on a grid corresponding to the experimental one. Figure 7 presents the experimental field (left column) and the numerical simulations (right column) in the transverse direction x as a function of the time at five different distances z from the tip of the cusp (-100, -50, 0, 50, and 100 mm). The agreement between the two series of fields is very good, in particular near the symmetry axis. The main differences between the experimental and the simulated fields are located off axis. Far away from the tip of the cusp (100 mm before), the wavefront is converging and its amplitude in the transverse direction is quite homogeneous. The closer to the tip the wavefront is, the stronger at the center of the beam the amplitude is. This is due to the focusing effects. At the tip and slightly after it, the beam is narrow and 100 mm after the tip it is clearly diverging.

Figure 8 displays the amplitude at 1 MHz measured on

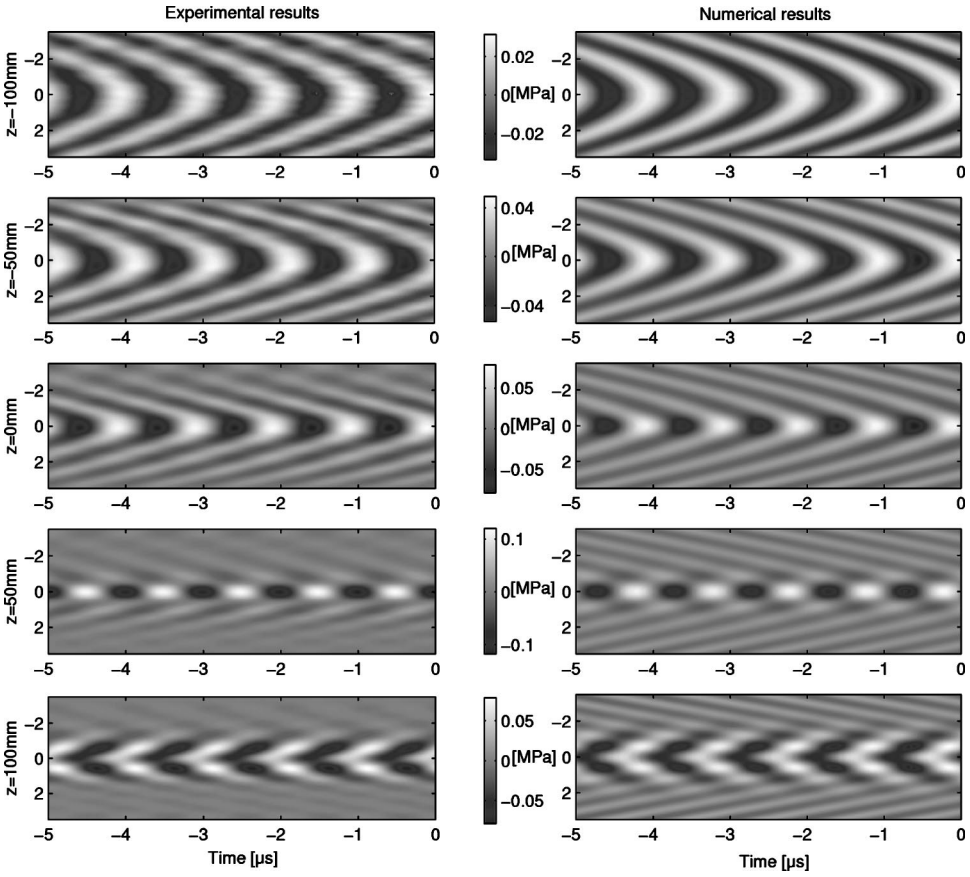

FIG. 7. Comparison between measured (left column) and numerically simulated (right column) pressure field in linear regime as a function of time (horizontal variable) and transverse variable x (vertical variable) at five different distances $z=-100$, -50, 0, 50, and 100 mm (gray levels: pressure levels).

each point of the scan grid in grayscale (black corresponds to zero and white corresponds to high intensity), compared to the contours of the Pearcey function (dashed white lines, with the same color levels). The agreement is still very good, especially near the Oz axis. The position and the amplitude of the main lobe are well recovered. The positions of the

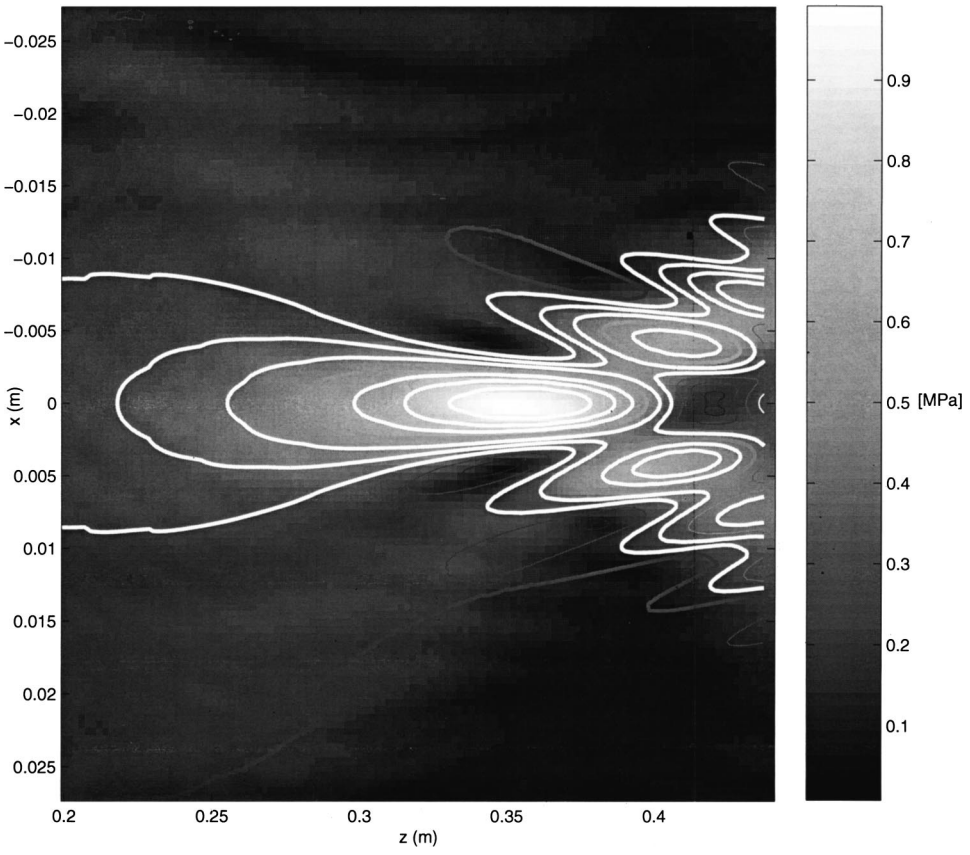

FIG. 8. Comparison between measured pressure field and the theoretical Pearcey function (white contour lines) in linear regime (gray levels: pressure levels).

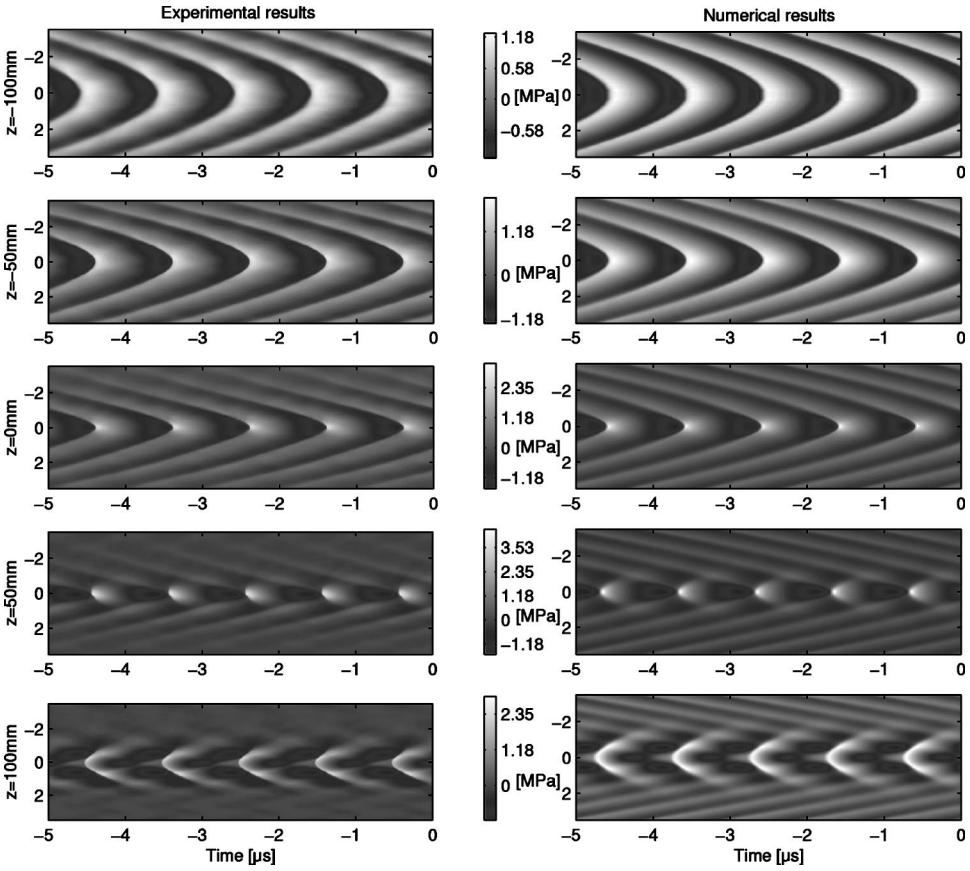

FIG. 9. Comparison between measured (left column) and numerically simulated (right column) pressure field in nonlinear regime as a function of time (horizontal variable) and transverse variable x (vertical variable) at five different distances $z=-100$, -50, 0, 50, and 100 mm (gray levels: pressure levels).

secondary lobes are matching relatively well but the amplitudes of the experimental measurements are lower than the simulated ones. These results confirm that the experimental setup is only usable near the Oz axis because of the finite size of the emitting array. Nevertheless, these results show that the experimental setup associated with the inverse filter technique permits the synthesis of a cusped caustic in the linear regime of 2-D space.

To study the focusing of weak shock waves at a cusped caustic, the previous computed signals by inverse filter technique are now emitted with high amplitude. Because of the high amplitude, nonlinear effects take place during the propagation between the array of transducers and the caustic cusp. The nonlinear effects induce a steepening of the temporal profile of the waves in accordance with the laws of nonlinear acoustics. The shock formation distance being shorter than the distance between the array of transducers and the cusped caustic, the incoming signal has shocks before tangenting the caustic. Once the high amplitude signals are emitted, the pressure is measured on the same grid as in linear regime but with a temporal sampling of 250 MHz. The results are given in Fig. 9 (left column), which shows the pressure fields in the transverse direction x as function of the time at five different locations z from the tip of the caustic (-100, -50, 0, 50, and 100 mm). The five images are different from those of the linear case (Fig. 7). Far before the caustic (-100 mm), the amplitude distribution is homogeneous and the shocks appear to be formed as indicated by the sharp transitions between black and white. As for the linear case, -50 mm away from the tip, the focusing effects increase the amplitude of the center of the beam. At the tip of the cusp the transverse size of the beam is narrower than in the linear case. Moreover, the compression phases (white areas) are shorter in time than the expansion ones (black areas), and the positive peaks are higher than the negative ones. This asymmetric waveform distorsion is well-known to result from a combination of diffraction and nonlinearity effects (see, for instance, Hamilton, 1998, p. 258).

The maximal overpressure is 66.82×10^5 Pa peak/peak (48.94×10^5 Pa for the positive part and 17.87×10^5 Pa for the negative one). It is detected on the Oz axis, 35 mm after the tip of the cusp. For a plane wave, the maximum overpressure at this distance is 10×10^5 Pa peak/peak. The amplification coefficient defined as the ratio between the overpressure in the focused case and the overpressure for a plane wave is consequently of 6.68. If only the positive part is taken into account, the amplification coefficient becomes 9.78. This coefficient is greater than for a fold caustic for which the corresponding values are respectively about 1.9 (peak to peak) and 3.8 (amplification of the positive part only). Moreover, note that this value of the amplification coefficient for a cusped caustic is in agreement with the value of about 9 found by Wanner *et al.* (1972) for sonic boom.

The numerical simulations in nonlinear regime require two input arguments which are extracted from the experimental results: the waveform of the incoming function and the nonlinear coefficient μ. The waveform of the incoming function is directly extracted from the experimental data on the Oz axis 100 mm before the tip of the cusp (sufficiently far before the cusp). The temporal profile for one period is given in Fig. 10 (dash line). The signal carries a shock which

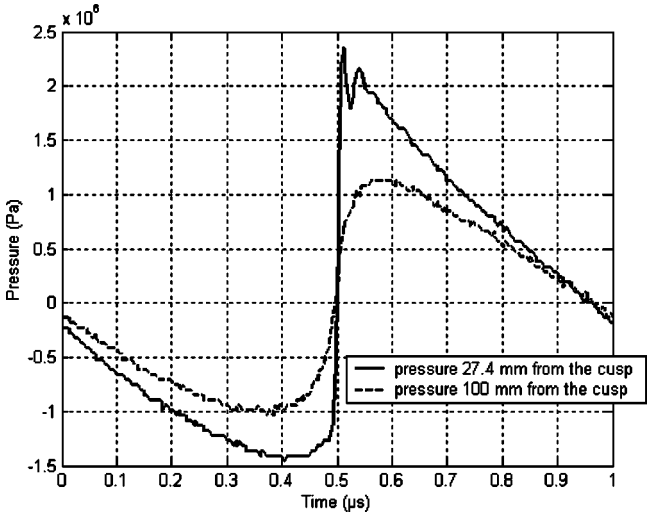

FIG. 10. Incoming signal (one period) measured at one boundary layer (-27.4 mm, solid line) and at -100 mm (dash line) from the tip of the cusped caustic in nonlinear regime.

is practically formed (the rise time is about 80 ns). The nonlinear coefficient $\mu=\beta(p_0/\rho_0 c_0^2)(k_0 a/27)^{1/2}$ [Eq. (8)] is calculated from the value of the pressure measured 27.4 mm before the tip of the caustic (distance equal to one diffraction length L_z), in agreement with theory. Note that the two inputs for the numerical code are extracted at two different ranges. At that distance, the pressure is 39.5×10^5 Pa and the shock is saturated with a measured rise time of 15 ns [Fig. 10 (solid line)]. Consequently, the value of the nonlinear coefficient is $\mu=0.35$. The numerical simulations are made with those two input arguments for a numerical grid corresponding to the experimental one. The results are given in Fig. 9 (right column). The agreement with the experimental results is excellent, especially around the Oz axis as in the previous comparisons. These results prove that the numerical solver simulates the physical reality with a good precision. Figure 11 shows the pressure (in Pa) as a function of the time (in μs) on the Oz axis at four different distances from the tip of the caustic (-100, -28, 0, and 100 mm); the solid lines are the experimental results while the dashed lines are the simulated ones. The numerical simulations fit the experimental results with a very good precision since the amplification level and the shock positions are recovered. Nevertheless, there is a little disagreement for the rise time, which is longer in the simulations than in the experiments. This may be due to numerical dissipation occurring during the resolution of the diffraction part. Indeed, while the numerical solver for Burgers' equation is a shock fitting algorithm, the method used to solve the linear KZ equation is a shock capturing algorithm. Shocks are not treated explicitly as such in the linear, diffraction part of the split-step algorithm. The finite differences automatically stabilize the algorithm by introducing numerical viscosity, which artificially increases the rise time.

CONCLUSION AND OUTLOOKS

A new explanation about the wavefront unfolding effect sometimes associated with acoustical shock waves incoming

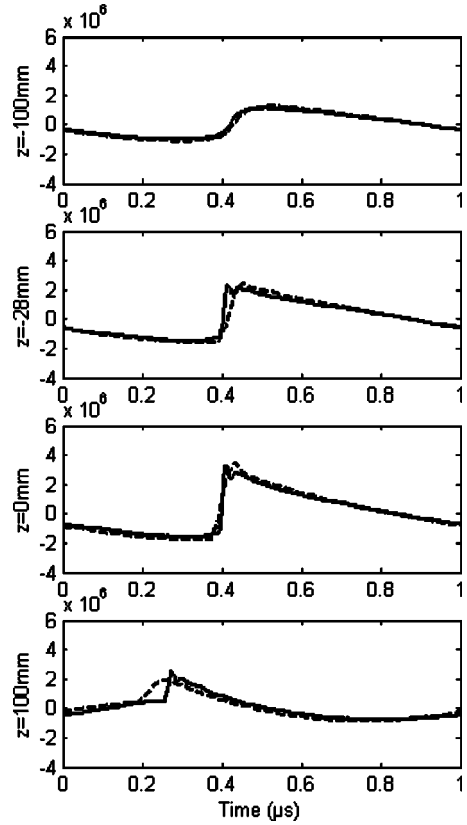

FIG. 11. Comparisons between measured (solid lines) and simulated (dash lines) pressure waveforms (in Pa) in nonlinear regime on the axis $x=0$ at four different distances from the tip of the cusped caustic ($z=-100$, -28, 0, and 100 mm).

on a cusped caustic has been proposed through original theoretical and numerical studies. This effect does not seem to be intrinsically nonlinear as expected by previous authors but associated both with nonlinearities and the geometry of the wavefront. Quantitative comparisons between numerical simulations and experimental results have demonstrated the validity of the theoretical modeling and the accuracy of the numerical code. Besides, as the numerical code is validated both experimentally and numerically, it is now possible to use it to simulate other configurations than those used in the experiments. In particular, it is interesting to apply this code to the prediction of sonic boom focusing in the case of complex aircraft maneuvers, that is to say, the focusing of an "N" wave at a cusped caustic. Figure 12 presents the time dependence of the pressure at three different locations near the cusp ($\bar{z}=0$, $\bar{x}=0$ for case a, $\bar{z}=1$, $\bar{x}=0.45$ for case b and $\bar{z}=2$, $\bar{x}=0.8$ for case c) for a nonlinearity parameter $\mu=0.1$ and an incoming "N" wave [$F(\tau)=-\tau$ if $|\tau|<1$,0 else]. On the tip of the caustic [Fig. 12(a)], the signal has no precursor and it begins with a steep shock. The second signal [Fig. 12(b)] displays a structure with two shocks visible at the beginning of the signal (noted 1 and 2 on the figure). The amplitude is weaker than on the Oz axis since the focusing effects are less important off axis. The structure of the signal [Fig. 12(c)] is made of three shocks associated with the interaction of three different signals in accordance with the theory which stipulates that in zone II three rays (and consequently three signals) pass through each point. Therefore, it

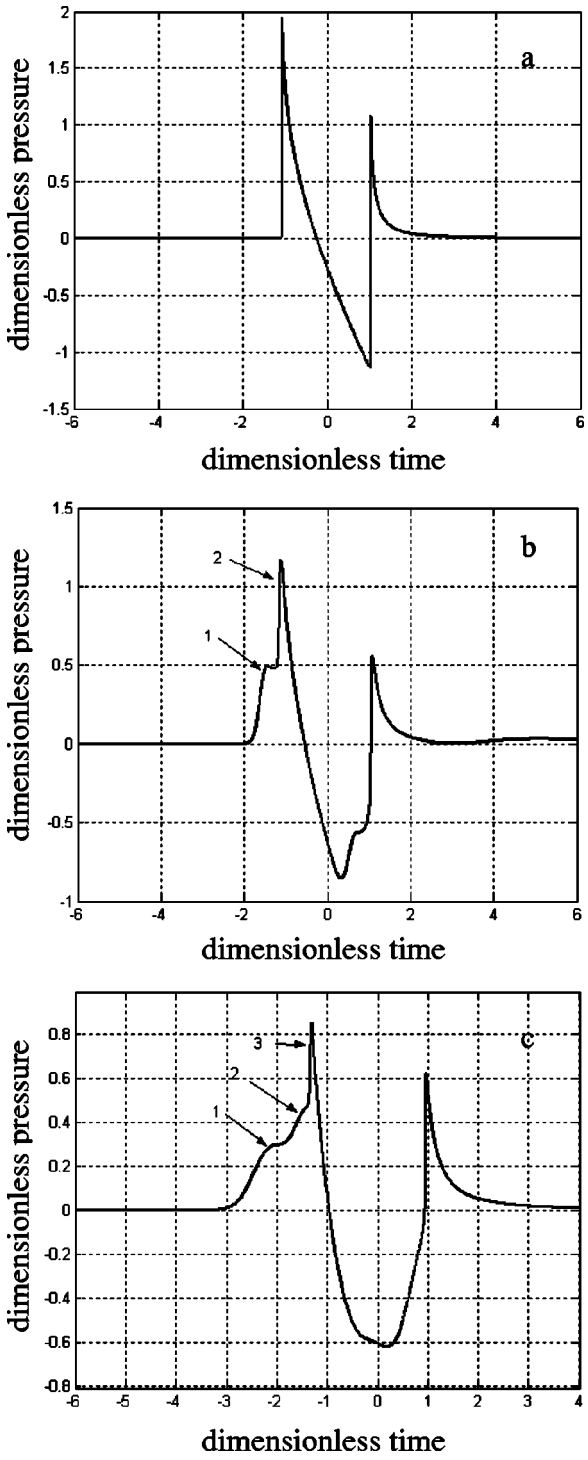

FIG. 12. Numerical simulations of the pressure time waveforms at three points near the cusped caustic cusp [(a) $\bar{z}=0$, $\bar{x}=0$; (b) $\bar{z}=1$, $\bar{x}=0.45$; and (c) $\bar{z}=2$, $\bar{x}=0.8$] for an "N" wave in nonlinear regime ($\mu=0.1$).

is possible to compare the numerical results with existing experimental measurements of sonic boom focusing. In particular, we can notice that the waveform obtained numerically in cases *a* and *b* corresponds to the waveforms already observed by Wanner *et al.* (1972, Fig. 15, microphones 17, 18 and 19 and Fig. 16 microphone 13) in the case of a supersonic aircraft entering into turn. Those results are another qualitative validation of the numerical code. Note that no signal with the characteristic of Fig. 12(c) has been recorded by Wanner *et al.* (1972), since no measurement has been performed inside the branch of the cusped caustic where the corresponding point lies. Also noticeable is the magnitude order of amplification in the experimental setup: around 3 for a fold caustic and 9 for a cusp caustic, the same magnitude orders as measured for sonic boom. Finally, complex waveforms as illustrated by Fig. 12 indicate caustics of higher order than the fold caustics may play an important role for explaining messy waveforms observed for sonic boom in the turbulent atmospheric boundary layer.

Considering the importance of the geometry effect on the focusing process as demonstrated in Sec. III, it would be desirable to improve the links between the aircraft maneuvers and the geometry of the cusped caustic. For real atmospheres, this would imply in particular to generalize the theoretical model to a 3D heterogeneous and moving medium, a task far from easy.

ACKNOWLEDGMENTS

This investigation have been carried out under a contract awarded by the European Commission, Contract No. G4RD-CT-2000-00398.

APPENDIX: THE NUMERICAL CODE

1. Presentation of the numerical method

To our knowledge, only one previous study is dedicated to the numerical simulation of the focusing of shock waves at a cusped caustic (Piacsek, 1995), based on the NPE equation [nonlinear paraxial equation (McDonald and Kuperman, 1987)]. This numerical study has been applied to investigate distortion of a sonic boom rippled wavefront (Piacsek, 2002), in order to validate the Pierce and Maglieri (1972) model of sonic boom wavefront folding in a turbulent atmosphere. However, no quantitative validation was presented. Here, relying on catastrophe theory and Guiraud scaling law, we are able to validate quantitatively the numerical resolution, before comparing it with experiments.

The theoretical model being based on the KZ equation, we have modified an algorithm solving the KZ equation previously used to study the nonlinear Fresnel diffraction of shock waves (Coulouvrat and Marchiano, 2003). That new algorithm solves the KZ equation [Eq. (7)] associated with the boundary conditions [Eq. (9)] in the temporal domain. The problem is formulated with the potential variable instead of the pressure. The potential is more suited to take into account shock waves. Indeed, a discontinuity for the pressure corresponds to an angular point for the potential. This approach has already been fruitful to solve the nonlinear Tricomi equation in the case of the focusing of weak shock waves at a fold caustic (Marchiano *et al.*, 2003a). The dimensionless potential is calculated from the dimensionless pressure:

$$\overline{p}=\frac{\partial\overline{\phi}}{\partial\overline{t}}. \tag{A1}$$

The KZ equation for the potential is

$$\frac{\partial^2\overline{\phi}}{\partial\overline{z}\partial\overline{t}}=\frac{\partial^2\overline{\phi}}{\partial\overline{x}^2}+\mu\frac{\partial}{\partial\overline{t}}\left(\frac{\partial\overline{\phi}}{\partial\overline{t}}\right)^2, \tag{A2}$$

Apart from the nonlinear term, this equation is identical to the equation for pressure [Eq. (7)]. The associated boundary conditions, valid only in zone I (Fig. 1), are

$$\overline{\phi}(\overline{x},\overline{z},\overline{t}) \xrightarrow[\sqrt{\overline{x}^2+\overline{z}^2}\to\infty]{} \frac{1}{\sqrt{|6\overline{\alpha}^2-\overline{z}|}} \times\int_{-\infty}^{\overline{t}} F(\overline{t}'+\overline{\alpha}\overline{x}+\overline{\alpha}^2\overline{z}-\overline{\alpha}^4)d\overline{t}'. \tag{A3}$$

The problem is symmetrical about the propagation axis Oz. Therefore it is possible to solve the problem for only one-half of the plane Oxz, in order to reduce the size of the computational domain. So the following symmetry condition is added to the boundary conditions [Eq. (16)]:

$$\frac{\partial}{\partial\overline{x}}\overline{\phi}(\overline{x}=0,\overline{z},\overline{t})=0. \tag{A4}$$

Note that these boundary conditions correspond to the cusped caustic and can be changed. To treat the real wavefront in Sec. III, a wavefront similar to the one used by Piacsek (2002) has been computed in the initial plane and nonlinear plane waves are used for the other boundary conditions.

In order to calculate the numerical solutions of the problem, the space variables are discretized on a regular grid. The points are equally spaced in the $\overline{z}$ direction starting from plane $\overline{Z}^-$ to plane $\overline{Z}^+$ with a step $\Delta\overline{z}$. They are also equally spaced in the $\overline{x}$ direction from 0 to $\overline{X}^+$ with a step $\Delta\overline{x}$. The time is discretized with a step $\Delta\overline{t}$.

The KZ equation [Eq. (15)] is solved plane after plane following the $\overline{z}$ direction. For each $\Delta\overline{z}$, the numerical solutions of the KZ equation are computed using the split-step method (Ames, 1977). This scheme has been widely used to solve the KZK [acronym of Khokhlov–Zabolotskaya–Kuznetsov, see Kuznetsov (1970)] equation which is a KZ equation taking into account the attenuation [see Hamilton (1998) for a review]. The split-step scheme consists in splitting the KZ equation into two simpler equations. The first one takes into account the diffraction. It is the linear KZ equation:

$$\frac{\partial^2\overline{\phi}}{\partial\overline{z}\partial\overline{t}}=\frac{\partial^2\overline{\phi}}{\partial\overline{x}^2}. \tag{A5}$$

The second one deals with the nonlinear effects. It is the Burgers equation for the potential:

$$\frac{\partial^2\overline{\phi}}{\partial\overline{z}\partial\overline{t}}=\mu\frac{\partial}{\partial\overline{t}}\left(\frac{\partial\overline{\phi}}{\partial\overline{t}}\right)^2. \tag{A6}$$

At each plane, first the linear KZ equation is solved numerically by an implicit finite differences scheme in the time domain based on the Lee and Hamilton scheme (1995). This scheme has originally been developed to solve the KZ equation for pressure in the framework of the beam propagation. It can easily be adapted to solve the KZ equation for potential since these two equations have the same form. Only the boundary conditions are different. Once the solution of the linear KZ is computed, it is used to initialize the calculation of the solution of the Burgers equation for potential on an elementary step $\Delta\overline{z}$. That solution is calculated semi-analytically with the Hayes graphical method (1969), which was recently adapted for the numerical procedure by Coulouvrat and Marchiano (2003) and Marchiano *et al.* (2003a). Finally, on a $\Delta\overline{z}$ step, the solution takes into account the diffraction and the nonlinear effects. The coupling between diffraction and nonlinearity is assured by the repetition of the procedure plane after plane. Note that, as the solution of the linear KZ equation, the solution of the Burgers equation is obtained in the temporal domain so that the whole resolution is achieved in the time domain. Moreover, there is no stability condition necessary to solve the Burgers equation (the solution is semi-analytical) or the linear KZ equation (the scheme is fully implicit). Finally, the pressure is calculated from Eq. (14) by a second-order finite differences scheme applied to the potential solution and a symmetry about the axis of propagation Oz permits to recover the pressure on the whole domain.

2. Validation of the algorithm

According to Guiraud's scaling for the cusped caustic [see Sec. III and Coulouvrat (2000)], if the incoming function is a step shock, the following quantities are constant for the point where the pressure is maximal: $\overline{p}_{\max}/\mu^{-1/3}=C_p$, $\overline{t}_{\max}/\mu^{4/3}=C_t$, $\overline{x}_{\max}/\mu=C_x$ and $\overline{z}_{\max}/\mu^{2/3}=C_z$, where $\overline{p}_{\max}$ represents the value of the maximal pressure, $\overline{t}_{\max}$ is the time for which the pressure is maximal, $\overline{x}_{\max}$, $\overline{z}_{\max}$ is the position where the pressure is maximal, and C_p, C_t, C_x and C_t are constants. These similitude laws are a good way to check the numerical code quantitatively, as they imply a strong coupling between nonlinearity and diffraction. Figure 13 shows that the numerical results are in very good agreement with the theoretical predictions. Indeed, the four ratios are practically constant for the values of μ greater than 0.02. This agreement shows that the amplitude of the peaks is limited and follows the similitude law $\tilde{p}_{\max}\mu^{-1/3}$. For the values of the nonlinear parameter under the threshold $\mu=0.02$, the results are not so good because the nonlinear effects are too small and the numerical resolution would require a more refined mesh grid than the one used. This result provides a quantitative validation of the numerical procedure. This kind of validation has already been used to validate a numerical code solving the nonlinear Tricomi equation with the Guiraud similitude law (Auger and Coulouvrat, 2002; Marchiano *et al.*, 2003a). Nevertheless, the results of those works were not in a such good agreement as the present ones, especially concerning the similitude law following the temporal variable. The very good agreement obtained in the

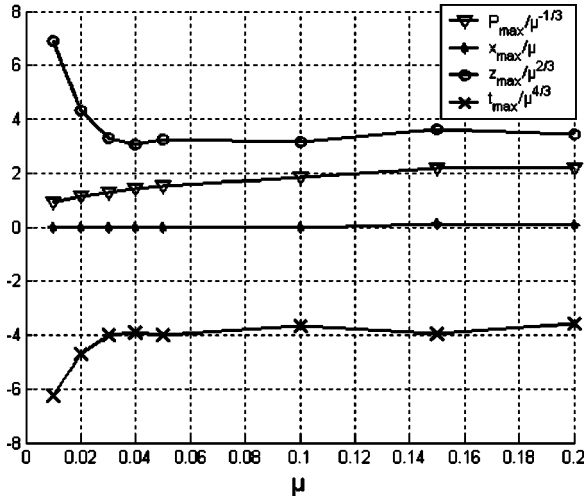

FIG. 13. Numerical check of theoretical Guiraud's similitude law.

present work is due to the fact that the numerical solver is now entirely in the time domain, contrarily to the case of the resolution of the nonlinear Tricomi equation for which the diffraction equation is solved in the frequency domain. This difference is important because for an algorithm in the time domain, it is possible to impose in the boundary condition an incoming step function to check the similitude law, whereas it is impossible for the nonlinear Tricomi solver, for which only artificially periodic incoming signals are available. The use of an algorithm in the frequency domain for the nonlinear Tricomi equation was required by the mixed elliptic/hyperbolic type of the equation, while the KZ equation is fully hyperbolic.

Finally, we indicate that a modified version of the present code has already been used to confirm theoretical predictions in a study about the nonlinear Fresnel diffraction of weak shock waves (Coulouvrat and Marchiano, 2003). In that previous study, the numerical code was similar to the code presented here except for the boundary conditions. The agreement between theoretical predictions and numerical results on self-similar solutions of the nonlinear KZ equation also permitted us to validate quantitatively the numerical method.

Ames, W. F. (**1977**). *Numerical Methods for Partial Differential Equations* (Academic, New York), pp. 315–467.

Auger, T., and Coulouvrat, F. (**2002**). ''Numerical simulation of sonic boom focusing,'' AIAA J. **40**, 1726–1734.

Berry, M. V. (**1976**). ''Waves and Thom's theorem,'' Adv. Phys. **25**, 1–26.

Coulouvrat, F. (**2000**). ''Focusing of weak acoustic shock waves at a caustic cusp,'' Wave Motion **32**, 233–245.

Coulouvrat, F., and Marchiano, R. (**2003**). ''Nonlinear Fresnel diffraction of weak shock waves,'' J. Acoust. Soc. Am. **114**, 1749–1757.

Cramer, M. S. (**1981a**). ''Focusing of weak three-dimensional shock waves,'' AIAA J. **19**, 1363–1365.

Cramer, M. S. (**1981b**). ''Focusing of weak shock waves at an axisymmetric arête,'' J. Fluid Mech. **110**, 249–253.

Cramer, M. S., and Seebass, A. R. (**1978**). ''Focusing of weak shock waves at an arête,'' J. Fluid Mech. **88**, 209–222.

Davy, B. A., and Blackstock, D. T. (**1971**). ''Measurements of the refraction and diffraction of a short *N* wave by a gas-filled soap bubble,'' J. Acoust. Soc. Am. **49**, 732–737.

Downing, M., Zamot, N., Moss, C., Morin, D., Wolski, E., Chung, S., Plotkin, K., and Maglieri, D. (**1998**). ''Controlled focused sonic booms from maneuvering aircraft,'' J. Acoust. Soc. Am. **104**, 112–121.

Gill, P. M., and Seebass, A. R. (**1973**). ''Nonlinear acoustic behavior at a caustic: an approximate analytical solution,'' AIAA Aeroacoustics Conference, Seattle (MIT, Cambridge), AIAA Paper 73-1037, pp. 353–386.

Guiraud, J.-P. (**1965**). ''Acoustique géométrique, bruit balistique des avions supersoniques et focalisation (Geometrical acoustics, balistic noise of supersonic aircraft and focusing),'' J. Mec. **4**, 215–267 (in French).

Hamilton, M. F. (**1998**). ''Sound beams,'' in *Nonlinear Acoustics*, edited by M. F. Hamilton and D. T. Blackstock (Academic, San Diego), pp. 233–261.

Hayes, W. D., Haefeli, R. C., Kulsrud, H. E. (**1969**). ''Sonic boom propagation in a stratified atmosphere with computer program,'' NASA CR-1299.

Kuznetsov, V. P. (**1970**). ''Equations of nonlinear acoustics,'' Sov. Phys. Acoust. **16**, 467–470.

Lee, Y.-S., and Hamilton, M. F. (**1995**). ''Time-domain modeling of pulsed finite-amplitude sound beams,'' J. Acoust. Soc. Am. **97**, 906–917.

Marchiano, R., Coulouvrat, F., and Grenon,, R. (**2003a**). ''Numerical simulation of shock wave focusing at fold caustics, with application to sonic boom,'' J. Acoust. Soc. Am. **114**, 1758–1771.

Marchiano, R., Thomas, J.-L., and Coulouvrat, F. (**2003b**). ''Experimental simulation of supersonic superboom in a water tank: nonlinear focusing of weak shock waves at a fold caustic,'' Phys. Rev. Lett. **91**(18), 184301(1-4).

Marston, P. L. (**1988**). ''Wavefront geometries giving transverse cusp and hyperbolic umbilic foci in acoustic shocks,'' in *Shock Waves in Condensed Matter 1987*, edited by S. C. Schmidt and N. C. Holmes (Elsevier, Amsterdam).

Marston, P. L. (**1992**). ''Geometrical and catastrophe optics methods in scattering,'' in *High Frequency and Pulse Scattering, Physical Acoustics*, edited by A. D. Pierce and R. N. Thurston (Academic, San Diego), Vol. XXI, pp. 1–234.

McDonald, B. E., and Kuperman, W. A. (**1987**). ''Time domain formulation for pulse propagation including nonlinear behavior at a caustic,'' J. Acoust. Soc. Am. **81**, 1406–1417.

Pearcey, T. (**1946**). ''The structure of an electromagnetic field in the neighbourhood of a cusp of a caustic,'' Philos. Mag. **37**, 311–317.

Piacsek, A. A. (**1995**). ''A numerical study of a weak step shocks that focus in two dimensions,'' Ph.D. thesis, Pennsylvania State University.

Piacsek, A. A. (**2002**). ''Atmospheric turbulence conditions leading to focused and folded sonic boom wave fronts,'' J. Acoust. Soc. Am. **111**, 520–529.

Pierce, A. D. (**1971**). ''Maximum overpressures of sonic boom near the cusp of caustics,'' in *Noise and Vibration Control Engineering*, edited by M. J. Crocker (Purdue U. P., West Lafayette), pp. 478–487.

Pierce, A. D., and Maglieri, D. J. (**1972**). ''Effects of atmospheric irregularities on sonic boom propagation,'' J. Acoust. Soc. Am. **51**, 702–721.

Plotkin, K. J., and Cantril, J. M. (**1976**). ''Prediction of sonic boom at focus,'' AIAA Paper 76-2, AIAA 14th Aerospace Sciences Meeting, Washington.

Prasad, P., and Sangeeta, K. (**1999**). ''Numerical simulation of converging nonlinear wavefronts,'' J. Fluid Mech. **385**, 1–20.

Sanaï, M., Toong, T. Y., and Pierce, A. D. (**1976**). ''Ballistic range experiments on superboom generated at increasing flight Mach numbers,'' J. Acoust. Soc. Am. **59**, 520–524.

Sturtevant, B., and Kulkarny, V. A. (**1976**). ''The focusing of weak shock waves,'' J. Fluid Mech. **73**, 651–671.

Tanter, M., Thomas, J.-L., and Fink, M. (**2000**). ''Time reversal and inverse filter,'' J. Acoust. Soc. Am. **108**, 223–234.

Thom, R. (**1972**). *Stabilité structurelle et morphogenèse* (Benjamin, Reading), pp. 72–107 (in French); English translation: *Structural stability and morphogenesis* (Benjamin, Reading, 1975).

Wanner, J.-C., Vallée, J., Vivier, C., and Théry, C. (**1972**). ''Theoretical and experimental studies of the focus of sonic booms,'' J. Acoust. Soc. Am. **52**, 13–32.

Whitham, G. B. (**1956**). ''On the propagation of weak shock waves,'' J. Fluid Mech. **1**, 290–318.

Zabolotskaya, E. A., and Khokhlov, R. V. (**1969**). ''Quasi-plane waves in the nonlinear acoustics of confined beams,'' Sov. Phys. Acoust. **15**, 35–40.